NeuroImage: Clinical 20 (2018) 731–741

Contents lists available at ScienceDirect

NeuroImage: Clinical

journal homepage: www.elsevier.com/locate/ynicl

Cerebrospinal fluid volumetric net flow rate and direction in idiopathic normal pressure hydrocephalus

Erika Kristina Lindstrøm[a,1], Geir Ringstad[b,c,1], Kent-Andre Mardal[a,d], Per Kristian Eide[c,e,*]

[a] Department of Mathematics, Faculty of Mathematics and Natural Sciences, University of Oslo, Norway
[b] Division of Radiology and Nuclear Medicine, Department of Radiology, Oslo University Hospital - Rikshospitalet, Oslo, Norway
[c] Institute of Clinical Medicine, Faculty of Medicine, University of Oslo, Oslo, Norway
[d] Department of Numerical Analysis and Scientific Computing, Simula Research Laboratory, Oslo, Norway
[e] Department of Neurosurgery, Oslo University Hospital, Rikshospitalet, Oslo, Norway

ARTICLE INFO

Keywords:
Cerebrospinal fluid
Phase-contrast MRI
Cranio-cervical junction
Cerebral aqueduct
Intracranial pressure

ABSTRACT

The aim of the present study was to examine cerebrospinal fluid (CSF) volumetric net flow rate and direction at the cranio-cervical junction (CCJ) and cerebral aqueduct in individuals with idiopathic normal pressure hydrocephalus (iNPH) using cardiac-gated phase-contrast magnetic resonance imaging (PC-MRI). An in-depth, pixel-by-pixel analysis of regions of interest from the CCJ and cerebral aqueduct, respectively, was done in 26 iNPH individuals, and in 4 healthy subjects for validation purposes. Results from patients were compared with over-night measurements of static and pulsatile intracranial pressure (ICP). In iNPH, CSF net flow at CCJ was cranially directed in 17/22 as well as in 4/4 healthy subjects. Estimated daily CSF volumetric net flow rate at CCJ was 6.9 ± 9.9 L/24 h in iNPH patients and 4.5 ± 5.0 L/24 h in healthy individuals. Within the cerebral aqueduct, the CSF net flow was antegrade in 7/21 iNPH patients and in 4/4 healthy subjects, while it was retrograde (i.e. towards ventricles) in 14/21 iNPH patients. Estimated daily CSF volumetric net flow rate in cerebral aqueduct was 1.1 ± 2.2 L/24 h in iNPH while 295 ± 53 mL/24 h in healthy individuals. Magnitude of cranially directed CSF net flow in cerebral aqueduct was highest in iNPH individuals with signs of impaired intracranial compliance. The study results indicate CSF flow volumes and direction that are profoundly different from previously assumed. We hypothesize that spinal CSF formation may serve to buffer increased demand for CSF flow through the glymphatic system during sleep and during deep inspiration to compensate for venous outflow.

1. Introduction

The choroid plexus is considered a major production site for the cerebrospinal fluid (CSF) that circulates through the ventricular system and subarachnoid space (Spector et al., 2015). Contributions to intraventricular CSF production may also come from the ependyma and parenchyma (McComb, 1983). In addition to provide mechanical protection and maintain the electrolytic environment and acid-base balance (Tumani et al., 2018), the discovery of the paravascular pathway proposed a potentially more important role of the CSF; namely a clearance of metabolic waste throughout the brain (Iliff et al., 2012; Lundgaard et al., 2017; Plog et al., 2015) and to drive lymphatic efflux of waste molecules from the craniospinal compartment (Ma et al., 2017).

Potential sites of extra-ventricular CSF production have been less explored, but have traditionally been considered of only minor importance compared to the amount secreted by choroid plexus (reviewed by (Brinker et al., 2014)). It may, however, be hypothesized that a substantial proportion of CSF may be produced outside the ventricular compartment and from a non-choroidal source. Late-onset hydrocephalus of chronic type due to aqueductal occlusion, which in principle represents an exclusion of supra-aqueductal choroid plexus from the subarachnoid compartment, is a well-known entity (Locatelli et al., 2014; Tisell et al., 2000), as well as chronic obstructive hydrocephalus

Abbreviations: AQP4, aquaporin 4; CCJ, cranio-cervical junction; CSF, cerebrospinal fluid; FOV, field of view; ICP, intracranial pressure; iNPH, idiopathic normal pressure hydrocephalus; MWA, mean wave amplitude; PC-MRI, phase-contrast magnetic resonance imaging; ROI, region of interest; SNR, signal-to-noise-ratio; TR, repetition time; TE, echo time

* Corresponding author at: Department of Neurosurgery, Oslo University Hospital, Rikshospitalet, Pb 4950 Nydalen, N-0424 Oslo, Norway.
E-mail addresses: p.k.eide@medisin.uio.no, peide@ous-hf.no (P.K. Eide).

[1] These authors contributed equally to this work.

https://doi.org/10.1016/j.nicl.2018.09.006
Received 9 August 2018; Received in revised form 6 September 2018; Accepted 11 September 2018
Available online 14 September 2018
2213-1582/ © 2018 The Author(s). Published by Elsevier Inc. This is an open access article under the CC BY-NC-ND license (http://creativecommons.org/licenses/BY-NC-ND/4.0/).

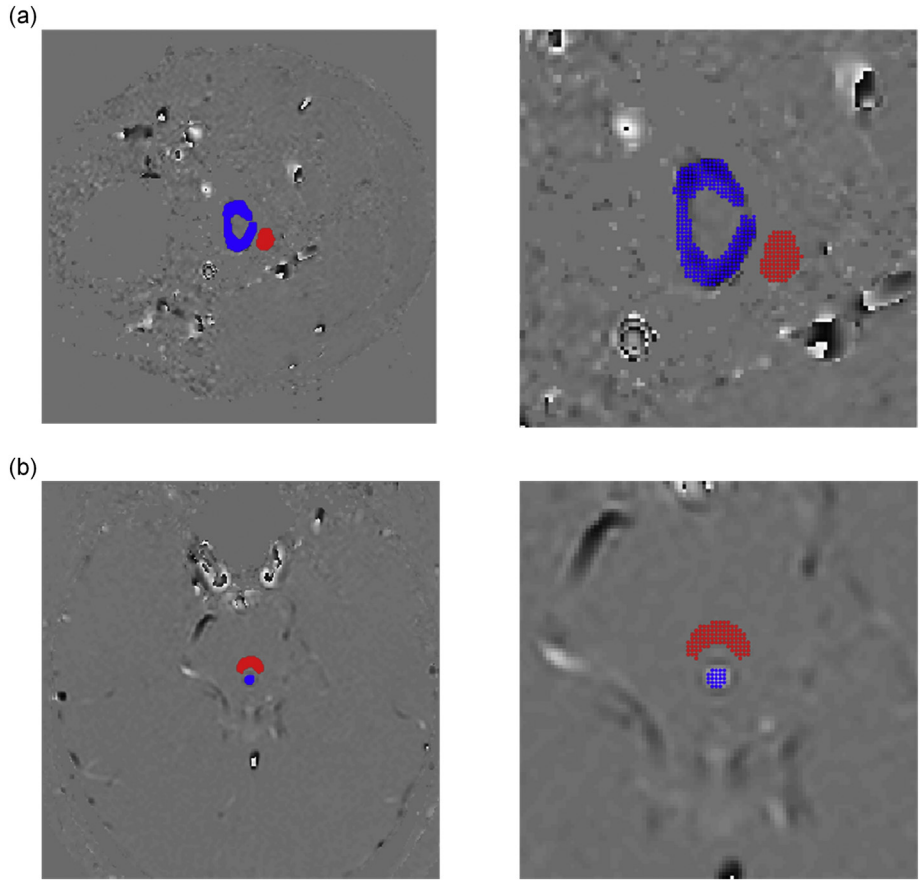

Fig. 1. The CCJ and cerebral aqueduct regions of interest in an iNPH individual (ID7). The ROIs are shown in blue and reference ROIs in red for (a) the CCJ and (b) the cerebral aqueduct. To the right is shown a zoomed in picture of the ROIs of the (a) CCJ and (b) cerebral aqueduct.

(Greitz, 2004). Studies reporting net retrograde aqueductal flow in hydrocephalus (Penn et al., 2011; Ringstad et al., 2016) are also implicating that CSF has to be produced by an extra-choroidal source. Some studies even suggest that the CSF production from the brain parenchyma is most important (Igarashi et al., 2014).

The question of CSF production within the spinal canal has been inadequately investigated. One study reported high rates of ependymal fluid secretion from the spinal cord ependyma (Sonnenberg et al., 1967). Recently, it was also reported previously unrecognized outflow pathway for fluids from perivascular spaces throughout the entire spinal cord (Lam et al., 2017).

While phase-contrast magnetic resonance imaging (PC-MRI) has previously been applied for quantification of ventricular CSF formation at the aqueductal level (Huang et al., 2004), the technique has yet not been used with the primary aim to assess CSF volumetric net flow rate and direction between the anatomically very different spinal canal and intracranial compartments. Here, CSF net flow in the upwards direction at the craniocervical junction (CCJ) would support a hypothesis that CSF is produced within the spinal canal.

The purpose of this study was to apply an in-depth analysis of PC-MRI data incorporating a pixel-by-pixel based approach to assess CSF volumetric net flow rate and direction at the CCJ and cerebral aqueduct of patients with idiopathic normal pressure hydrocephalus (iNPH). Healthy subjects were also included to validate the PC-MRI measurements.

2. Materials and methods

2.1. Ethical approvals

The Regional Committee for Medical and Health Research Ethics of Health Region South-East, Norway (S-07237) and the Institutional Review Board of Oslo university hospital (07/5869) approved this study. The study participants were included after written and oral informed consent. Study design was prospective and observational.

2.2. Patients

2.2.1. iNPH patients

The study included consecutive patients with probable idiopathic normal pressure hydrocephalus (iNPH), as defined by the American-European guidelines (Relkin et al., 2005). They were referred to the Department of neurosurgery, Oslo University Hospital - Rikshospitalet, Oslo, Norway, from local neurological departments, based on clinical symptoms and findings indicative of iNPH, and imaging findings of ventriculomegaly. Within the Department of neurosurgery, they were clinically assessed, and clinical severity graded based on a previously described NPH grading scale (Eide and Sorteberg, 2010; Eide and Sorteberg, 2016). Selection criteria for CSF diversion surgery were based on a combination of clinical symptoms and findings indicative of iNPH, imaging findings, co-morbidity, and results of intracranial pressure (ICP) monitoring, as previously described (Eide and Sorteberg, 2010; Eide and Sorteberg, 2016). The iNPH patients not meeting our selection criteria for shunt surgery were managed conservatively. Clinical response to shunt surgery was performed after 6–12 months by a person blinded to PC-MRI data.

2.2.2. Healthy subjects

Four healthy subjects underwent PC-MRI for validation of the CCJ and aqueductal CSF flow measurements. Each reference individual underwent five repeated MRI acquisitions to control for variability between repeated scans.

2.3. MRI acquisitions

The PC-MRI information from patients was acquired on a 3 Tesla (T) Philips Achieva (Philips Medical Systems, Best, The Netherlands) with a 16 channel head coil, and an acquisition plane perpendicular to the aqueduct with repetition time (TR) = 24 ms/echo time (TE) = 16 ms, voxel size 0.60 × 0.80 × 4.00 mm^3, matrix of 232 × 175 pixels, field of view (FOV) 14 cm, velocity encoding 10 cm/s, and 30–40 phases with retrospective peripheral cardiac gating. All MRI scans were obtained at day-time.

Healthy subjects were scanned in a Philips 3 T Ingenia system (Philips Medical Systems, Best, The Netherlands) with a 32 Channel head coil. All acquisition plane, level and parameters were set equally as for the patients.

2.4. Image analysis

2.4.1. Regions of interest

For both the CCJ and cerebral aqueduct, regions of interest (ROIs) were manually defined along the outer border of the CCJ (Fig. 1a) and cerebral aqueduct (Fig. 1b) by an experienced neuroradiologist (G.R.), using Philips Q-flow software (Philips Medical Systems, Best, The Netherlands). The ROIs were rather generous, and velocities were plotted every pixel (one cycle) to exclude pixels outside CSF. The neuroradiologist was blinded for information about clinical NPH-score and whether the patient had responded to shunting or not.

Thereafter, the velocities from each of the chosen pixels were carefully evaluated by plotting the pixel velocities in MATLAB. Any included pixel that displayed unexpected behavior (flow signal unlikely to represent physiological CSF flow) was excluded from the ROI in further processing by the assumption it would represent an artifact, or noise, not flow signal.

2.4.2. Velocities & aliasing

Recorded velocities were converted by linear transformation from pixel values to centimeters per second by applying the velocity encoding using MATLAB® (Mathworks, Natick, United States). Positive values are cranial direction and negative values are caudal direction. A filter corrected pixels that contained aliased velocities, e.g. velocities that exceeded the velocity encoding. The filter was activated if the temporal velocity difference in one pixel was larger than 1.1 times the velocity encoding. In that case the aliased pixel was replaced by $v = v_a \pm 2 \times V_{enc}$, where v is the filtered velocity, v_a is the aliased pixel value and V_{enc} is the velocity encoding. Two of the patients displayed pixels with values exceeding twice the velocity encoding, these were corrected by applying the filter a second time with the adjustment$v = v_a \pm 4 \times V_{enc}$.

2.4.3. Bias, SNR

A reference region of interest (reference ROI) was manually defined close to the original region of interest (Fig. 1a–b). The reference ROI contained 100–140 pixels in order to capture a potential bias in the data set and to quantify the noise level.

The recorded velocities in the reference ROI was converted to centimeters per second and thereafter averaged over the number of pixels to achieve a mean velocity of the noise. The calculated mean velocity was considered as bias in the data set. The original velocity data was corrected for biasing by subtracting the noise mean velocity from each pixel velocity in the region of interest.

The noise level was estimated by calculating the signal-to-noise ratio (SNR) defined as

$$SNR = 10 \times log\left(\frac{P_S}{P_N}\right)$$

where P_S is the power of the signal and P_N is the power of the noise (Power is defined as the amplitude squared). We defined the signal as the mean velocity in the original region of interest and calculated SNR for each pixel in the reference region of interest. This provides a number of 100–140 SNR values depending of the size of the reference ROI. To achieve one representative SNR for each data set, we average the calculated SNR numbers.

Suppl Fig.1 illustrates pixel and mean velocities in region of interest and reference ROI of the CCJ (Suppl Fig.1a) and cerebral aqueduct (Suppl Fig. 1b). The figures visualize a positive bias with SNR of 16 (Suppl Fig. 1a) and 32 (Suppl Fig. 1b) decibel. The variation in pixel and mean velocities between individuals are further illustrated in Suppl Fig.2a–f.

2.4.4. Volumetric flow calculations

Volumetric flow rate Q (ml/s) in the region of interest was calculated by computing the sum of each pixel velocity over one cycle multiplied with pixel size

$$Q(t) = \left(\sum_{i=1}^{n} v_i\right) \times dx \times dy$$

The positive and negative contributions of the volumetric flow rate were calculated separately in the same manner, but instead of summing all pixels in the ROI, the positive and negative velocities were extracted before the calculation. Bidirectional flow within the CCJ is visualized in Fig. 2b, and Fig. 3b shows bidirectional flow within the cerebral aqueduct. The 2D and 3D shows information that may get lost if the velocities over the ROI are averaged before calculating the volumetric flow rate.

The net volume over one cycle was calculated by discrete integration (trapezoidal method) of Q over time:

$$Net\ volume = \frac{dt}{2} \sum_{i=1}^{n} (Q(t_{i+1}) + Q(t_i))$$

Volumes over one cycle in cranial and caudal direction were calculated by integration of positive and negative volume fluxes over time. The CSF volumetric net flow rate (expressed in milliliter, mL) during one cycle (mL/cycle) was determined by the sum of the positive and negative CSF flux.

The MRI scan time was 6 min, during which the heart rate (HR) was determined. The daily CSF volumetric net flow rate, expressed in liter (L) per 24 h was estimated by multiplying the CSF net flow volume over one cardiac cycle with the HR and then multiplied with 1440 (minutes/day).

2.4.5. Net CSF stroke volume ratio

We calculated the ratio between the CSF volumetric net flow rate per cardiac cycle at the cerebral aqueduct versus the CCJ according to this formula:

$$\frac{Vol_A}{Vol_{CCJ}} \times 100$$

where Vol_A is the net volume of CSF flow during one cycle measured in the cerebral aqueduct and Vol_{CCJ} is the net volume of CSF flow during one cycle measured in CCJ. If net CSF flow is directed upwards, we consider this ratio to be an estimate of the portion of CSF that distributes from CCJ into the supra-aqueductal compartment during one cardiac cycle. Others have previously determined the ratio between average stroke volume at the aqueduct and CCJ levels, not considering net volumes (Baledent et al., 2004; Wagshul et al., 2006).

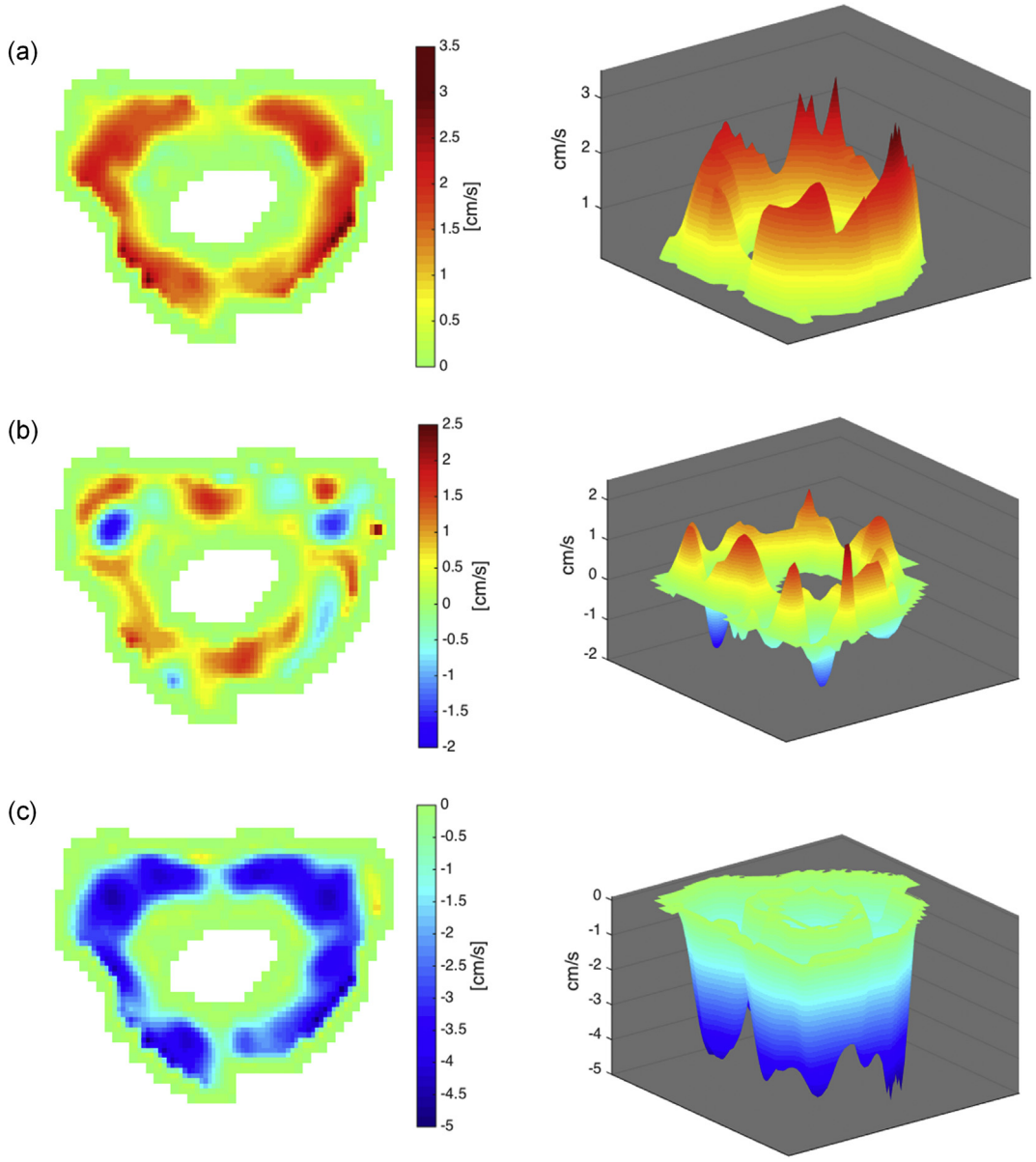

Fig. 2. Bidirectional CSF flow in CCJ of an iNPH patient (IDs 13). The CSF flow is presented in 2D and 3D showing (a) upward flow, (b) combined, and (c) downward flow.

2.4.6. Pressure gradients

The peak-peak pressure gradient was computed from the measured velocities by applying Navier-Stokes equations with the assumption of fluid flow perpendicular to the acquisition plane. A detailed description of the method has been previously presented (Ringstad et al., 2017a).

2.5. MRI biomarkers of hydrocephalus

The MRI of each individual was examined for biomarkers of hydrocephalus, including determination of Evan's index (Brix et al., 2017), callosal angel (Virhammar et al., 2014), and for the presence of disproportionately enlarged subarachnoid space hydrocephalus (DESH) (Hashimoto et al., 2010).

2.6. ICP measurements

Continuous monitoring of static and pulsatile ICP was done in all iNPH patients, as previously described in detail (Eide and Sorteberg, 2010). In short, an ICP sensor was placed in the brain parenchyma through a small burr hole in the scull in local anesthesia, and monitoring done over-night using a computerized system. While static ICP represents the absolute pressure difference between the intracranial compartment and reference atmospheric pressure, MWA is defined as the pressure difference between the systolic maximum and diastolic minimum pressures for cardiac-induced single ICP waves during consecutive 6-s time intervals. The mean ICP and MWA values were determined for the 6-s time windows from 23 p.m. to 7 a.m. (i.e. 4800 6-s time windows), including both the average of MWA, and the percentage of mean ICP $\geq$15 mmHg, and percentage of MWA $\geq$5 mmHg during the recording period. Threshold levels of MWA representing indication for shunting are MWA in average $\geq$ 4 mmHg (High-MWA) and/or percentage of MWA $\geq$5 mmHg in $\geq$10% of recording time (labeled "High MWA" subgroup) (Eide and Sorteberg, 2010).

2.7. Statistics

For the statistical analysis, we used SPSS version 22 (IBM Corporation, Armonk, NY). Differences between iNPH subgroups were

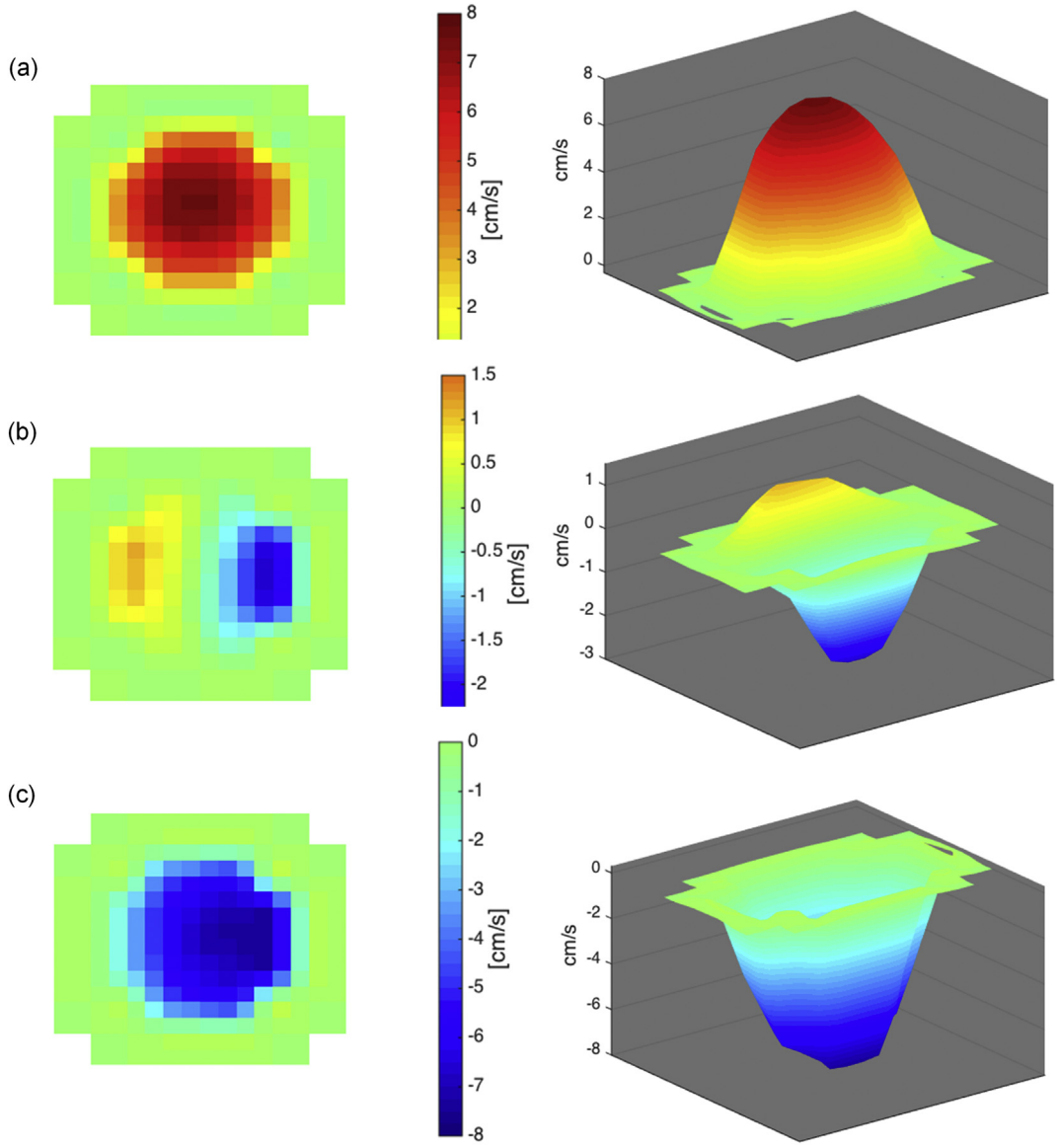

Fig. 3. Bidirectional CSF flow in cerebral aqueduct of an iNPH patient (IDs 13). The CSF flow is presented in 2D and 3D showing (a) upward flow, (b) combined, and downward flow (c).

determined by Mann-Whitney *U* test. Statistical significance was accepted at the 0.05 level (two-tailed).

3. Results

3.1. Patients

The study cohort included 26 individuals with probable iNPH. Four healthy subjects were included for validation purposes and imaged 5 times each. The demographic information for the patient cohort and healthy subjects is given in Table 1. Among the 26 iNPH patients, 17/19 had clinical improvement following shunt surgery. The 17 iNPH shunt-responders can be categorized as “definite iNPH”, as defined by the Japanese guidelines (Mori et al., 2012). The subgroup “Non-responders/Conservative” included 2 shunt non-responders and 7 managed conservatively without shunt. Suppl Table 1 provides information at the individual level.

3.2. Phase-contrast MRI estimated CSF volumes of CCJ and cerebral aqueduct

The PC-MRI-estimated CSF peak-to-peak pulse pressure gradient and CSF volumetric net flow rate at the individual level are presented in Suppl Table 2 for CCJ and in Suppl Table 3 for cerebral aqueduct. Technically acceptable PC-MRI measurements useful for our pixel-by-pixel based approach were obtained in 22/26 regarding CCJ and in 21/26 iNPH individuals regarding the cerebral aqueduct. Results of repeated MRI acquisitions in healthy reference individuals are given in Suppl Table 4 for CCJ and in Suppl Table 5 for cerebral aqueduct. For each individual, average of values from all single pixel analyses was determined. We compared net and mean stroke volumes (average of systolic and diastolic volumetric CSF flow) during one cardiac cycle. The size of region of interest and velocities are key numbers for calculations of volumes, and are therefore presented. Peak-to-peak pressure gradients influence the fluid flow and are also reported.

The CSF net flow for the CCJ had direction towards the cranial cavity in 17/22 (77%) and towards the spinal canal in 5/22 (23%) iNPH individuals, while it was cranially directed in all 4 healthy

Table 1
Demographic information, PC-MRI-derived CSF volumetric net flow rates and directions of the iNPH patients and healthy subjects, and ICP scores of the iNPH patients.

	Healthy	iNPH cohort	iNPH cohort		Significance[a]
			Responders	Non-responders/ Conservative	(Responders vs. Non-responders/ Conservative)
Demographic information					
N	4	26	17	9	
Age (yrs)	30.8 ± 8.5	69.8 ± 9.6	71.1 ± 7.8	67.4 ± 12.4	*ns*
Gender (F/M)	1/3	11/15	7/10	4/5	
MRI biomarkers					
Evan's index	0.26 ± 0.02	0.38 ± 0.05	0.39 ± 0.05	0.36 ± 0.04	*ns*
Callosal angle (degrees)	101.5 ± 8.4	88.7 ± 26.0	84.1 ± 25.6	97.4 ± 25.8	*ns*
DESH (N; %)	0 (0%)	13 (50%)	9 (53%)	4 (44%)	*ns*
PC-MRI-derived CSFvolumetric flow rate and direction at CCJ					
CSF volumetric net flow rate (mL/cycle)	0.081 ± 0.070	0.068 ± 0.10	0.073 ± 0.093	0.059 ± 0.121	*ns*
Estimated CSF volumetric net flow rate (L/24 h)	6.40 ± 4.88	6.86 ± 9.04	7.12 ± 8.10	6.31 ± 11.51	*ns*
Cranially directed net CSF flow (N)	4	17	12	5	*ns*
Spinally directed net CSF flow (N)	0	5	3	2	
PC-MRI-derived CSF volumetric flow rate and direction in cerebral aqueduct					
CSF volumetric net flow rate (mL/cycle)	−0.003 ± 0.001	0.012 ± 0.025	0.023 ± 0.021	−0.006 ± 0.02	*p = 0.020*
Estimated CSF volumetric net flow rate (L/24 h)	−0.26 ± 0.05	1.09 ± 2.24	2.141 ± 1.646	−0.65 ± 1.95	*p = 0.016*
Antegrade-directed net CSF flow (N)	4	7	3	4	*ns*
Retrograde-directed net CSF flow (N)	0	14	11	3	
Net CSF stroke volume ratio (aqueduct/CCJ; % ratio))	2.9 ± 2.2	23.4 ± 19.8	24.5 ± 20.0	20.7 ± 21.2	*p = 0.037*
ICP scores					
Static ICP					
Mean ICP average (mmHg)		6.6 ± 3.0	7.1 ± 2.6	5.8 ± 3.6	*ns*
Mean ICP > 15 mmHg (%)		1 ± 3	1 ± 4	2 ± 3	*ns*
Pulsatile ICP					
MWA average (mmHg)		4.8 ± 1.5	5.2 ± 1.3	4.0 ± 1.4	*p = 0.041*
MWA > 5 mmHg (%)		37 ± 34	46 ± 33	20 ± 32	*ns*

iNPH: idiopathic normal pressure hydrocephalus; CCJ: cranio-cervical junction; DESH: disproportionately enlarged subarachnoid space hydrocephalus; MWA: mean ICP wave amplitude.
[a] Significance determined by Mann-Whitney U test (ns: non-significant)

subjects (Suppl Table 2; Table 1). Regarding the cerebral aqueduct, the CSF net flow was antegrade in 7/21 (33%) and retrograde in 14/21 (67%) iNPH individuals, while antegrade in all 4 healthy subjects (Suppl Table 3; Table 1).

Concerning the repeated MRI acquisitions in 4 healthy individuals, the CSF net flow at CCJ was cranially directed in 17/20 observations (Suppl Table 4) and antegrade directed in cerebral aqueduct in 18/20 observations (Suppl Table 5).

Table 1 presents average CSF volumetric net flow rate and direction (positive values show net flow in the cranial direction) in CCJ and cerebral aqueduct during each cardiac cycle and over 24 h. The estimated CSF volumetric net flow rate in CCJ was 6.9 ± 9.0 L/24 h and 4.5 ± 5.0 L/24 h in iNPH and healthy individuals, respectively, while the estimated CSF volumetric net flow rate in cerebral aqueduct was 1.1 ± 2.2 L/24 h and 295 ± 53 mL/24 h in iNPH and healthy subjects, respectively. While there were no significant differences between shunt responders and the other iNPH cases in CCJ regarding net CSF flow during each cardiac cycle or over 24 h, the CSF volumetric net flow within the cerebral aqueduct over each cardiac cycle or during 24 h differed significantly between iNPH shunt responders and the others (Table 1). The MRI biomarkers of hydrocephalus, Evan's index, callosal angel and signs of DESH did not differ between shunt responders and the other iNPH cases.

The net CSF stroke volume ratio is a measure for intraventricular redistribution of CSF flow when being increased. As compared to healthy subjects, in whom this fraction was only 2.9%, this was 23.4% in the iNPH cohort (Table 1). The net CSF stroke volume ratio was significantly higher in iNPH shunt responders than in iNPH patients being treated conservatively or not responding to surgery (Table 1).

Fig. 4 provides a histogram presentation of the estimated CSF volumetric net flow rates over 24 h for the individual cases at the CCJ (Fig. 4a) and cerebral aqueductal (Fig. 4b) levels. The inter-individual variation and large volumetric flow rates should be noted.

3.3. ICP scores and CSF net volumes

The ICP scores of the iNPH patient cohorts are shown in Table 1 (ICP scores at individual level are presented in Suppl Table 6). While 17/17 shunt-responders and 1/2 shunt non-responders had MWA values above previously defined threshold levels (Eide and Sorteberg, 2010), the 7 conservatively managed iNPH patients had MWA values below threshold vales. Fig. 5 presents CSF volumetric net flow rates in CCJ (Fig. 5a) and cerebral aqueduct (Fig. 5b) for individuals with MWA above or below thresholds, i.e. MWA ≥ or < 4 mmHg on average during over-night monitoring. Positive volumetric flow rates indicate cranially directed CSF net flow. The cohort with MWA > thresholds is considered to have impaired intracranial compliance, i.e. reduced pressure-volume reserve capacity. In this cohort, the CSF volumetric net flow rate was not different within the CCJ (Fig. 5a), but was significantly higher within the cerebral aqueduct, indicating redistribution of CSF flow into the ventricles in patients with reduced intracranial compliance (Fig. 5b).

4. Discussion

In this in-depth analysis of PC-MRI data from the CCJ, we provide evidence that the spinal canal may serve as a net producer of CSF when iNPH patients as well as healthy subjects are in the supine position. Moreover, there was CSF net flow upwards the aqueduct and into the ventricles in iNPH patients, particularly in those with signs of reduced intracranial compliance. In healthy subjects, however, CSF flow was net downwards, or “antegrade”.

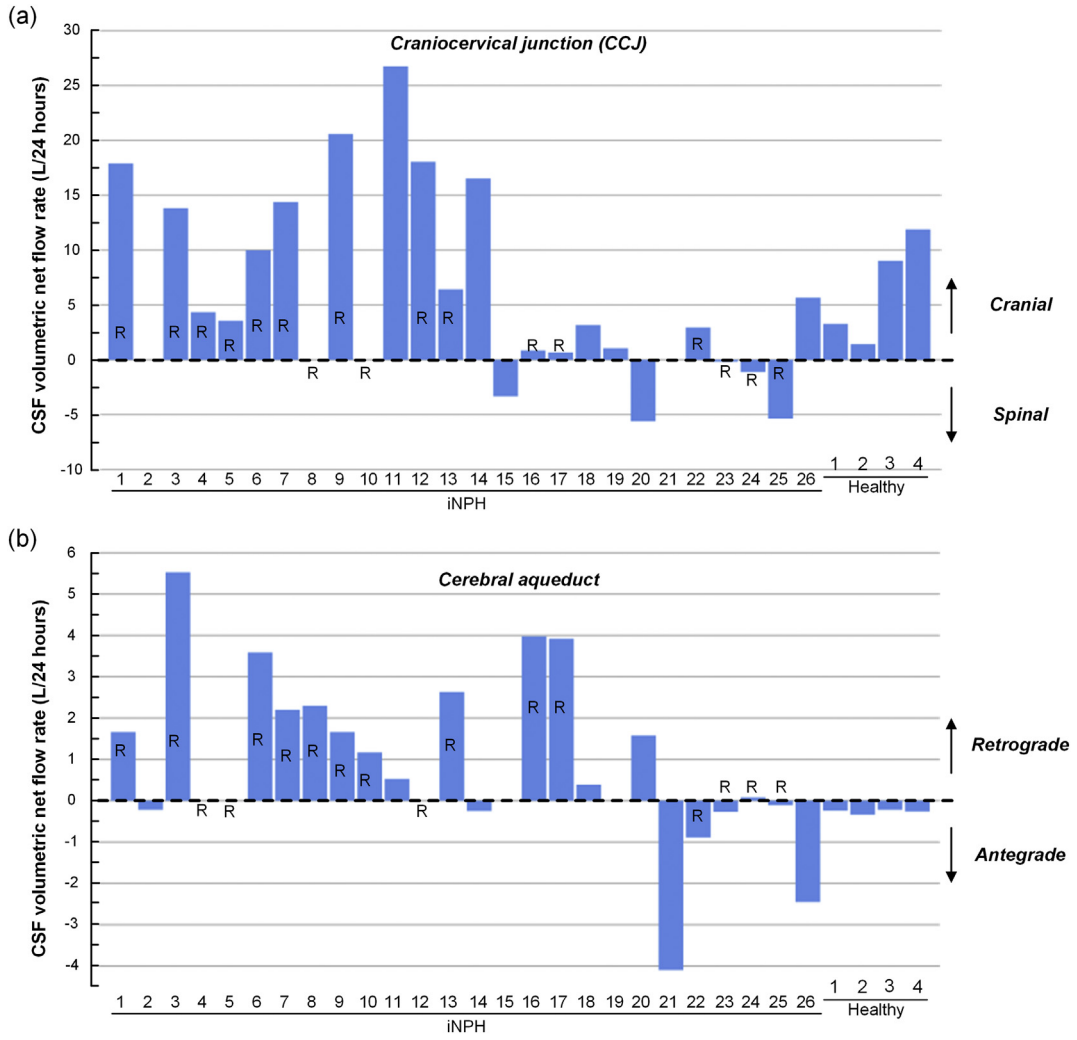

Fig. 4. Estimated CSF volumetric net flow rate in CCJ and cerebral aqueduct of iNPH patients and healthy subjects. The volume and direction of net CSF flow in (a) the CCJ and (b) cerebral aqueduct estimated for a 24 h interval is shown for the individual patients. Shunt responders are identified as R (Responders).

4.1. The spinal canal as net producer of CSF

The spinal subarachnoid space is in continuity with peri-arterial and peri-venous perivascular spaces of the spinal cord, which in their turn are continuous with the spinal cord extracellular space and basement membranes (Lam et al., 2017). This anatomical continuity between nervous tissue and the subarachnoid compartment allows for low resistance fluid exchange between these two compartments, which therefore should be possible to occur in both directions (Lam et al., 2017). CSF hydrostatic pressure is highly susceptible to body posture (Kajimoto et al., 2000). According to Starling mechanisms, body posture dependent CSF hydrostatic pressure increase within the spinal canal may therefore be a major determinant of whether the spinal cord paravascular compartment produces or resorbs fluid.

Our findings of CSF net flow into the cranial compartment are well in line with a previous, real-time MRI study, where net upwards CSF flow was observed during forced inspiration, occurring in conjunction with increased venous outflow through spinal epidural veins (Dreha-Kulaczewski et al., 2017), while the ensuing expiration lead to downward CSF flow only in the lower part of the spinal canal (Dreha-Kulaczewski et al., 2018). CSF inflow into the head may be regarded a necessity to balance inspiratory induced CSF outflow as the primary event. Such a compensatory mechanism would highly unlikely exist without the capacity for net CSF production within the spinal canal.

Other supporting evidence comes from in vivo observations of CSF tracer propagation within the spinal canal of supine human subjects, where intrathecally injected contrast agent at the lower lumbar level typically enters the posterior cranial fossa within 10–20 min (Ringstad et al., 2017b). Even though a hydrophilic tracer can propagate in a pulsating fluid without net flow by dispersion, the short spinal transit time that was observed makes the effect of merely dispersion less likely.

4.2. Intracranial CSF formation

Intracranial pressure (ICP) is also highly influenced by body posture (Schneider et al., 1993; Brosnan et al., 1985) and has been shown to increase from −14.2 mmHg in the sitting position to 4.6 mmHg in the supine position (Kajimoto et al., 2000). During night-time, ICP is also higher than at day-time (Eide and Sorteberg, 2010), suggesting an influence of sleep and circadian rhythm. As in the spinal cord, paravascular spaces of the brain are connected with the subarachnoid compartment (Bedussi et al., 2016), where an abundant amount of aquaporin-4 (AQP4) channels at astrocytic end feet surround blood vessels (Nagelhus and Ottersen, 2013). As there also occurs a continuous, bi-directional fluid exchange over the blood-brain barrier (Brinker et al., 2014), CSF production outside the choroid plexus has the potential to be vast. Previous invasive tests for measurement of CSF production may have significantly underestimated this, as they were typically performed by infusion of non-diffusible reference substances, chosen because of their ability of not being absorbed into capillaries

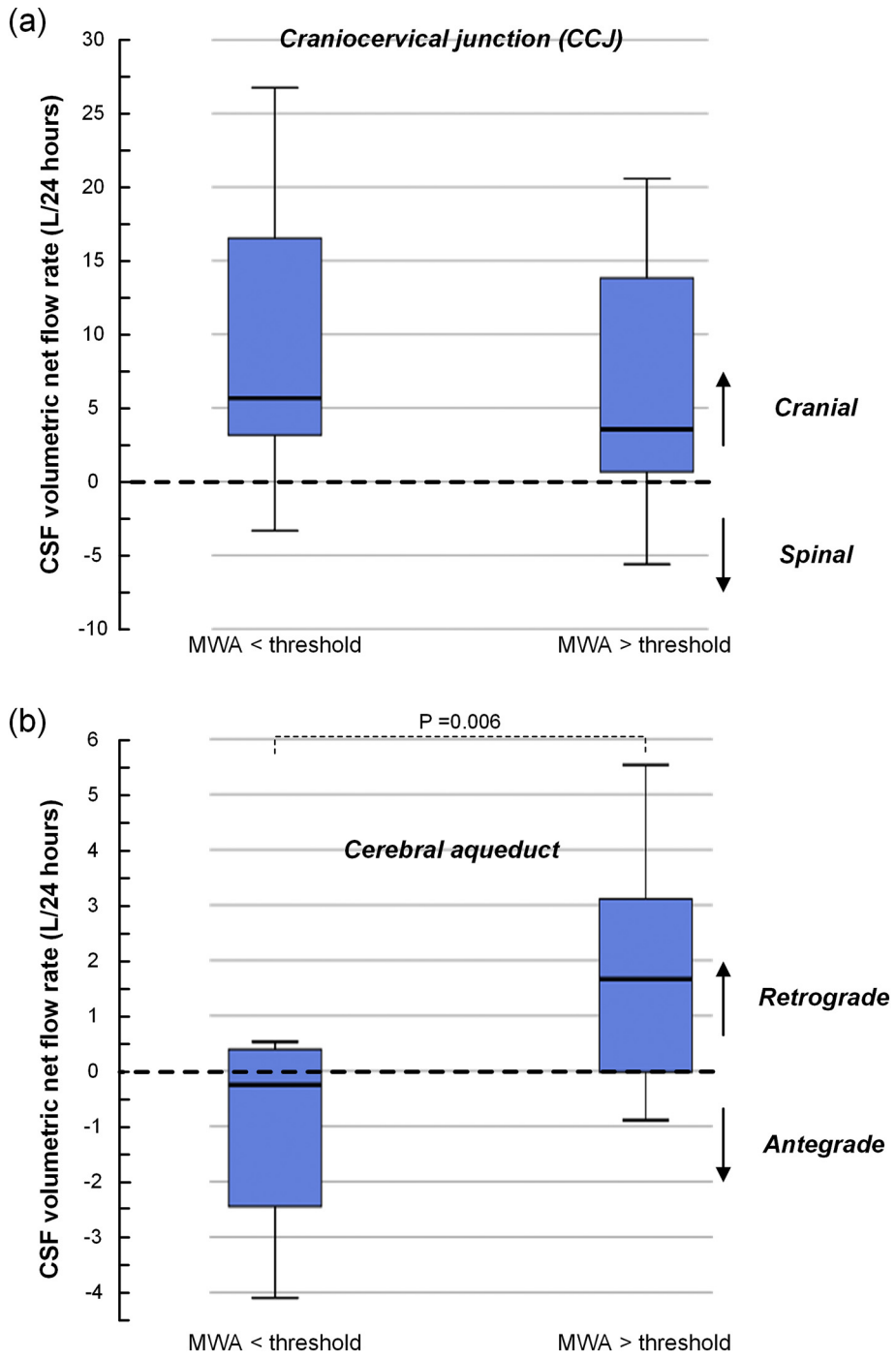

Fig. 5. Differences in estimated CSF volumetric net flow rates in CCJ and cerebral aqueduct between iNPH categories with different intracranial compliance indices. The volume and direction of CSF flow in (a) the CCJ and (b) cerebral aqueduct is present for iNPH categories with MWA below or above threshold values. MWA below threshold is indicative of normal intracranial compliance while MWA above threshold indicate impaired intracranial compliance. Differences between groups were determined by independent samples *t*-test.

(reviewed by (Bateman and Brown, 2012)). True CSF turnover rates may thereby have been substantially underestimated. Studies not in adherence with the previously accepted paradigm of CSF formation at a rate of approximately 0.3 ml/min, may have been discredited as flawed. For example, data from a study performed in 1952 (Bering Jr., 1952), which reported free and constant exchange of water between the blood, brain and CSF, was recalculated and found to imply a CSF formation rate of > 22 mL/min. The ventriculo-cisternal perfusion method (Pappenheimer technique) has also recently been heavily criticized for not being valid, and it has also been provided experimental evidence for CSF production to dominate outside the ventricular system (Oreskovic and Klarica, 2014). The present study observations of CSF net formation within the spinal canal in iNPH as well as healthy subjects question the validity of the Pappenheimer technique in assessing the total CSF production rate, as it is performed on the assumption that CSF is produced entirely within the ventricular system.

While this remains controversial (Spector et al., 2015), several authors have found that CSF production can be reduced as response to a pressure increase due to hydrocephalus (Johanson et al., 1999; Silverberg et al., 2002; Tulassay et al., 1990). A hypothesis that

intracranial CSF production may be decreased in the flat body posture, while increased within the spinal canal, seems therefore worth testing in future studies.

4.3. CSF flow at sleep

The natural body posture during rest and sleep is in the horizontal position.

The net contribution of CSF from the spinal canal to the intracranial compartment in supine subjects, as shown in this study, may well serve to buffer increased CSF demand in the resting, or sleep state. At sleep, the brain interstitial space expands significantly, accompanied by a steep increase of fluid exchange between the CSF and interstitial spaces (Xie et al., 2013) and enables a significantly reduced resistance for glymphatic clearance of macromolecules and bulk flow through the brain (own unpublished observations) (Iliff et al., 2012). In the more upright head position, glymphatic flow has also been proven directly to be less than in the flat supine or lateral position (Lee et al., 2015). Increased water content in the brain after sleep is underlined by the observation of increased brain volume after sleep (Trefler et al., 2016) and that increased diffusivity in the brain over-night is due to an increase in the volume fraction of CSF-like free-water (Thomas et al., 2018). A nearly fourfold increase in CSF production rate from day-time (12 mL/h) to night-time (42 mL/h) has been shown by flow analysis utilizing MRI (Nilsson et al., 1992), and CSF itself has been proposed to have a role in mediating regulation of the circadian rhythm (Myung et al., 2018).

4.4. Retrograde net CSF aqueductal flow in iNPH

In this study, net CSF flux into the supra-aqueductal ventricles was a typical feature of iNPH disease. Particularly, retrograde aqueductal flow was a feature of patients with increased intracranial pressure pulsatility above established threshold values (MWA > 4 mmHg), previously shown to highly predict a beneficial shunt response (Eide and Sorteberg, 2010; Eide and Sorteberg, 2016). This supports the hypotheses that choroid plexus CSF production may be down-regulated and be replaced by extra-ventricular sources. Unlike in healthy subjects, net retrograde aqueductal flow as phenomenon has been described in hydrocephalic patients in previous studies utilizing PC-MRI (Baledent et al., 2004; Bateman and Brown, 2012; Kim et al., 1999; Penn et al., 2011; Ringstad et al., 2016) and was recently also proven in iNPH patients that were followed during a 24 h time period with MRI after utilizing intrathecal MRI contrast agent as CSF tracer (Ringstad et al., 2017b). In the latter, contrast agent administered to CSF at the lumbar level entered the entire ventricular system, where it remained within the ventricles for a prolonged time period of at least 24 h and migrated through the ventricular ependyma and into brain tissue (Ringstad et al., 2017b). Net CSF flow into the ventricles would require a positive pressure change in the same direction, which has been considered sufficient to enlarge the ventricles (Levine, 2008; Linninger et al., 2005). It may be speculated that net flow upwards the aqueduct may be CSF taking the path of least resistance due to obstruction of paravascular CSF flow in iNPH, in which level of AQP4 and its anchoring protein Dystrophin-71 has been proven reduced (Eide and Hansson, 2018).

4.5. Methodological considerations and study limitations

Differences in shunt selection criteria may impact results of studies on iNPH. Independent of the criteria, a high proportion of shunt responders indicate that “true” iNPH patients are included. In the present iNPH group, 16/22 patients were shunt responders. The cohort may therefore in large be regarded to be representative of “true” iNPH, or as “definite iNPH”, as defined by the Japanese guidelines of iNPH (Mori et al., 2012).

Net CSF flow measurements yields volumetric data in the order of microliters and are prone to technical error. An important challenge is the subtraction of large quantities of flow in opposite directions (i.e. systolic and diastolic CSF flow) resulting in a much smaller net flow volume. In this, net flow volume may be within size of the measurement error and has in calculations of mean aqueductal stroke volume been subtracted (Bradley et al., 1996). Particularly at the CCJ, magnitude of CSF net flow demonstrated much larger variations than magnitude of average flow (stroke volume) for repeated scans (Suppl. Table 4).

The CSF volumetric net flow rates over 24 h were computed by multiplying HR with net volume over one cardiac cycle. Obviously, this approach represents a simplification as both the parameters net volume and HR may vary over 24 h. The MRI scan lasted about 6 min. This short time does not allow for long-term monitoring, which is a methodological weakness.

When using PC-MRI for net flow calculations in particular, the need for correction of background velocity offset has been emphasized, as errors are dependent on the specific settings of the equipment used at different sites (Gatehouse et al., 2010). Such phase offsets may be derived from eddy currents, concomitant gradients (Maxwell terms) and gradient field non-linearity's (Lorenz et al., 2014). In advance of this study, the scanner manufacturer had pre-installed a phase correction filter to correct for eddy current effects. Moreover, we corrected for baseline velocity offsets from adjacent, stationary tissue with a ROI of robust size (Fig.1). Such offset was demonstrated, but proved to be of limited size compared to the amounts of net flow (Suppl Fig. 1). The finding of opposite net flow directions in healthy subjects at the CCJ and aqueduct level, respectively, should further suggest that baseline velocity offset was not significant.

Spatial resolution is an important factor in PC-MRI measurements. Smaller pixel size reduces partial volume averaging from stationary tissue adjacent to CSF, and is particularly crucial at level of the aqueduct, which is of a much smaller area than the CSF space within the spinal canal at level of the CCJ. The pixel size used for the current study ($0.6 \times 0.8\ mm^2$) may be considered moderate, and within average used by other investigators (reviewed by (Ragunathan and Pipe, 2018)). After a per-pixel aliasing filter was applied as previously described (Ringstad et al., 2017a), we now also visually analyzed flow curves from every pixel overlapping with the aqueduct for signs of flow that could be considered not physiological or otherwise influenced by technical error. Such pixels were removed from the calculation of net flow. Also, 1/22 patients was excluded from the study due to extreme aliasing (3 times venc). We expect this in-depth analysis to have reduced influence from technical errors in the current PC-MRI measurements considerably.

Furthermore, CSF flow may also be heavily influenced by respiration, which is not controlled for during cardiac gated PC-MRI (Dreha-Kulaczewski et al., 2015). During inspiration, CSF flow at the level of the aqueduct and CCJ is net upwards, and directed oppositely during expiration. Yildiz et al. found that respiratory effects are averaged out at conventional, cardiac-gated PC-MRI compared to real-time PC-MRI (Yildiz et al., 2017). Furthermore, in a recent study, Spijkerman et al. used respiratory gated PC-MRI and found that net CSF flow quantity at the aqueductal level was affected by breathing in healthy subjects, but did not affect conclusion about net flow direction (Spijkerman et al., 2018).

Finally, another methodological weakness may be impact of variability of MRI acquisitions. Repeated scans are difficult in patients due to the discomfort of MRI scanning. In each of the healthy subjects, we performed five repeated scans to test for variability of PC-MRI acquisitions, which showed that the variability between scans was modest for both CCJ and aqueduct measurements (Suppl Tables 4 and 5).

5. Conclusions

In this study, an in-depth, pixel-by-pixel analysis of CSF flow from

PC-MRI revealed caudo-cranial net flow in the CCJ of supine iNPH patients and healthy subjects, and in the aqueduct of iNPH patients. Net CSF flow from the spinal canal in the supine position may serve to compensate for increased CSF demand at the long term through the glymphatic system during sleep, when the extracellular space expands, and at the short term during forced inspiration to compensate for increased venous outflow. Furthermore, redistribution of CSF flow from the subarachnoid compartment to the intraventricular space was highly associated with pathological intracranial pressure pulsatility in iNPH and may be a sign of increased resistance to paravascular CSF flow mediated by AQP4.

Supplementary data to this article can be found online at https://doi.org/10.1016/j.nicl.2018.09.006.

Funding

Department of Neurosurgery, Oslo University Hospital, Rikshospitalet, Oslo, Norway.

References

Baledent, O., Gondry-Jouet, C., Meyer, M.E., De Marco, G., Le Gars, D., Henry-Feugeas, M.C., Idy-Peretti, I., 2004. Relationship between cerebrospinal fluid and blood dynamics in healthy volunteers and patients with communicating hydrocephalus. Investig. Radiol. 39, 45–55.

Bateman, G.A., Brown, K.M., 2012. The measurement of CSF flow through the aqueduct in normal and hydrocephalic children: from where does it come, to where does it go? Childs Nerv. Syst. 28, 55–63.

Bedussi, B., van der Wel, N.N., de Vos, J., van Veen, H., Siebes, M., Vanbavel, E., Bakker, E.N., 2017 Apr. Paravascular channels, cisterns, and the subarachnoid space in the rat brain: a single compartment with preferential pathways. J. Cereb. Blood Flow Metab. 37 (4), 1374–1385. https://doi.org/10.1177/0271678X16655550. (Epub 2016 Jan 1).

Bering Jr., E.A., 1952. Water exchange of central nervous system and cerebrospinal fluid. J. Neurosurg. 9, 275–287.

Bradley, W.G.,.Jr., Scalzo, D., Queralt, J., Nitz, W.N., Atkinson, D.J., Wong, P., 1996. Normal-pressure hydrocephalus: evaluation with cerebrospinal fluid flow measurements at MR imaging. Radiology 198, 523–529.

Brinker, T., Stopa, E., Morrison, J., Klinge, P., 2014. A new look at cerebrospinal fluid circulation. Fluids Barriers CNS 11, 10.

Brosnan, R.J., Steffey, E.P., LeCouteur, R.A., Imai, A., Farver, T.B., Kortz, G.D., 1985. Effects of body position on intracranial and cerebral perfusion pressures in isoflurane-anesthetized horses. J. Appl. Physiol. 92 (6), 2542–2546 (2002 Jun).

Brix, M.K., Westman, E., Simmons, A., Ringstad, G.A., Eide, P.K., Wagner-Larsen, K., Page, C.M., Vitelli, V., Beyer, M.K., 2017. The Evans' Index revisited: New cut-off levels for use in radiological assessment of ventricular enlargement in the elderly. Eur. J. Radiol. 95, 28–32.

Dreha-Kulaczewski, S., Joseph, A.A., Merboldt, K.D., Ludwig, H.C., Gartner, J., Frahm, J., 2015. Inspiration is the major regulator of human CSF flow. J. Neurosci. 35, 2485–2491.

Dreha-Kulaczewski, S., Joseph, A.A., Merboldt, K.D., Ludwig, H.C., Gartner, J., Frahm, J., 2017. Identification of the Upward Movement of Human CSF in Vivo and its Relation to the Brain Venous System. J. Neurosci. 37, 2395–2402.

Dreha-Kulaczewski, S., Konopka, M., Joseph, A.A., Kollmeier, J., Merboldt, K.D., Ludwig, H.C., Gartner, J., Frahm, J., 2018. Respiration and the watershed of spinal CSF flow in humans. Sci. Rep. 8, 5594.

Eide, P.K., Hansson, H.A., 2018. Astrogliosis and impaired aquaporin-4 and dystrophin systems in idiopathic normal pressure hydrocephalus. Neuropathol. Appl. Neurobiol. 44, 474–490.

Eide, P.K., Sorteberg, W., 2010. Diagnostic intracranial pressure monitoring and surgical management in idiopathic normal pressure hydrocephalus: a 6-year review of 214 patients. Neurosurgery 66, 80–91.

Eide, P.K., Sorteberg, W., 2016. Outcome of surgery for idiopathic normal pressure hydrocephalus: Role of preoperative static and pulsatile intracranial pressure. World Neurosurg 86 (186–193), e181.

Gatehouse, P.D., Rolf, M.P., Graves, M.J., Hofman, M.B., Totman, J., Werner, B., Quest, R.A., Liu, Y., von Spiczak, J., Dieringer, M., Firmin, D.N., van Rossum, A., Lombardi, M., Schwitter, J., Schulz-Menger, J., Kilner, P.J., 2010. Flow measurement by cardiovascular magnetic resonance: a multi-Centre multi-vendor study of background phase offset errors that can compromise the accuracy of derived regurgitant or shunt flow measurements. J. Cardiovasc. Magn. Reson. 12, 5.

Greitz, D., 2004. Radiological assessment of hydrocephalus: new theories and implications for therapy. Neurosurg. Rev. 27, 145–165 (discussion 166-147).

Hashimoto, M., Ishikawa, M., Mori, E., Kuwana, N., 2010. Diagnosis of idiopathic normal pressure hydrocephalus is supported by MRI-based scheme: a prospective cohort study. Cerebrospinal Fluid Res. 7, 18.

Huang, T.Y., Chung, H.W., Chen, M.Y., Giiang, L.H., Chin, S.C., Lee, C.S., Chen, C.Y., Liu, Y.J., 2004. Supratentorial cerebrospinal fluid production rate in healthy adults: quantification with two-dimensional cine phase-contrast MR imaging with high temporal and spatial resolution. Radiology 233, 603–608.

Igarashi, H., Tsujita, M., Kwee, I.L., Nakada, T., 2014. Water influx into cerebrospinal fluid is primarily controlled by aquaporin-4, not by aquaporin-1: 17O JJVCPE MRI study in knockout mice. Neuroreport 25, 39–43.

Iliff, J.J., Wang, M., Liao, Y., Plogg, B.A., Peng, W., Gundersen, G.A., Benveniste, H., Vates, G.E., Deane, R., Goldman, S.A., Nagelhus, E.A., Nedergaard, M., 2012. A paravascular pathway facilitates CSF flow through the brain parenchyma and the clearance of interstitial solutes, including amyloid beta. Sci. Transl. Med. 4, 147ra111.

Johanson, C.E., Szmydynger-Chodobska, J., Chodobski, A., Baird, A., McMillan, P., Stopa, E.G., 1999. Altered formation and bulk absorption of cerebrospinal fluid in FGF-2-induced hydrocephalus. Am. J. Phys. 277, R263–R271.

Kajimoto, Y., Ohta, T., Miyake, H., Matsukawa, M., Ogawa, D., Nagao, K., Kuroiwa, T., 2000. Posture-related changes in the pressure environment of the ventriculoperitoneal shunt system. J. Neurosurg. 93, 614–617.

Kim, D.S., Choi, J.U., Huh, R., Yun, P.H., Kim, D.I., 1999. Quantitative assessment of cerebrospinal fluid hydrodynamics using a phase-contrast cine MR image in hydrocephalus. Childs Nerv. Syst. 15, 461–467.

Lam, M.A., Hemley, S.J., Najafi, E., Vella, N.G.F., Bilston, L.E., Stoodley, M.A., 2017. The ultrastructure of spinal cord perivascular spaces: Implications for the circulation of cerebrospinal fluid. Sci. Rep. 7, 12924.

Lee, H., Xie, L., Yu, M., Kang, H., Feng, T., Deane, R., Logan, J., Nedergaard, M., Benveniste, H., 2015 Aug 5. The Effect of Body Posture on Brain Glymphatic Transport. J. Neurosci. 35 (31), 11034–11044. https://doi.org/10.1523/JNEUROSCI.1625-15.2015.

Levine, D.N., 2008. Intracranial pressure and ventricular expansion in hydrocephalus: have we been asking the wrong question? J. Neurol. Sci. 269, 1–11.

Linninger, A.A., Tsakiris, C., Zhu, D.C., Xenos, M., Roycewicz, P., Danziger, Z., Penn, R., 2005. Pulsatile cerebrospinal fluid dynamics in the human brain. IEEE Trans. Biomed. Eng. 52, 557–565.

Locatelli, M., Draghi, R., A, D.I.C., Carrabba, G., Zavanone, M., Pluderi, M., Spagnoli, D., Rampini, P., 2014. Third Ventriculostomy in Late-onset Idiopathic Aqueductal Stenosis Treatment: a Focus on Clinical Presentation and Radiological Diagnosis. Neurol. Med. Chir. (Tokyo) 54, 1014–1021.

Lorenz, R., Bock, J., Snyder, J., Korvink, J.G., Jung, B.A., Markl, M., 2014. Influence of eddy current, Maxwell and gradient field corrections on 3D flow visualization of 3D CINE PC-MRI data. Magn. Reson. Med. 72, 33–40.

Lundgaard, I., Lu, M.L., Yang, E., Peng, W., Mestre, H., Hitomi, E., Deane, R., Nedergaard, M., 2017. Glymphatic clearance controls state-dependent changes in brain lactate concentration. J. Cereb. Blood Flow Metab. 37, 2112–2124.

Ma, Q., Ineichen, B.V., Detmar, M., Proulx, S.T., 2017. Outflow of cerebrospinal fluid is predominantly through lymphatic vessels and is reduced in aged mice. Nat. Commun. 8, 1434.

McComb, J.G., 1983. Recent research into the nature of cerebrospinal fluid formation and absorption. J. Neurosurg. 59, 369–383.

Mori, E., Ishikawa, M., Kato, T., Kazui, H., Miyake, H., Miyajima, M., Nakajima, M., Hashimoto, M., Kuriyama, N., Tokuda, T., Ishii, K., Kaijima, M., Hirata, Y., Saito, M., Arai, H., 2012. Guidelines for management of idiopathic normal pressure hydrocephalus: second edition. Neurol. Med. Chir. 52, 775–809.

Myung, J., Schmal, C., Hong, S., Tsukizawa, Y., Rose, P., Zhang, Y., Holtzman, M.J., De Schutter, E., Herzel, H., Bordyugov, G., Takumi, T., 2018. The choroid plexus is an important circadian clock component. Nat. Commun. 9, 1062.

Nagelhus, E.A., Ottersen, O.P., 2013. Physiological roles of aquaporin-4 in brain. Physiol. Rev. 93, 1543–1562.

Nilsson, C., Stahlberg, F., Thomsen, C., Henriksen, O., Herning, M., Owman, C., 1992. Circadian variation in human cerebrospinal fluid production measured by magnetic resonance imaging. Am. J. Phys. 262, R20–R24.

Oreskovic, D., Klarica, M., 2014. Measurement of cerebrospinal fluid formation and absorption by ventriculo-cisternal perfusion: what is really measured? Croatian Med. J. 55, 317–327.

Penn, R.D., Basati, S., Sweetman, B., Guo, X., Linninger, A., 2011. Ventricle wall movements and cerebrospinal fluid flow in hydrocephalus. J. Neurosurg. 115, 159–164.

Plog, B.A., Dashnaw, M.L., Hitomi, E., Peng, W., Liao, Y., Lou, N., Deane, R., Nedergaard, M., 2015. Biomarkers of traumatic injury are transported from brain to blood via the glymphatic system. J. Neurosci. 35, 518–526.

Ragunathan, S., Pipe, J.G., 2018 Apr. Radiofrequency saturation induced bias in aqueductal cerebrospinal fluid flow quantification obtained using two-dimensional cine phase contrast magnetic resonance imaging. Magn. Reson. Med. 79 (4), 2067–2076. https://doi.org/10.1002/mrm.26883. (Epub 2017 Aug 22).

Relkin, N., Marmarou, A., Klinge, P., Bergsneider, M., Black, P.M., 2005. Diagnosing idiopathic normal-pressure hydrocephalus. Neurosurgery 57, S4–16 (discussion ii-v).

Ringstad, G., Emblem, K.E., Eide, P.K., 2016. Phase-contrast magnetic resonance imaging reveals net retrograde aqueductal flow in idiopathic normal pressure hydrocephalus. J. Neurosurg. 124, 1850–1857.

Ringstad, G., Lindstrom, E.K., Vatnehol, S.A.S., Mardal, K.A., Emblem, K.E., Eide, P.K., 2017a. Non-invasive assessment of pulsatile intracranial pressure with phase-contrast magnetic resonance imaging. PLoS One 12, e0188896.

Ringstad, G., Vatnehol, S.A.S., Eide, P.K., 2017b. Glymphatic MRI in idiopathic normal pressure hydrocephalus. Brain 140, 2691–2705.

Schneider, G.H., von Helden, G.H., Franke, R., Lanksch, W.R., Unterberg, A., 1993. Influence of body position on jugular venous oxygen saturation, intracranial pressure and cerebral perfusion pressure. Acta Neurochir. Suppl. (Wien) 59, 107–112.

Silverberg, G.D., Huhn, S., Jaffe, R.A., Chang, S.D., Saul, T., Heit, G., Von Essen, A., Rubenstein, E., 2002. Downregulation of cerebrospinal fluid production in patients with chronic hydrocephalus. J. Neurosurg. 97, 1271–1275.

Sonnenberg, H., Solomon, S., Frazier, D.T., 1967. Sodium and chloride movement into the

central canal of cat spinal cord. Proc. Soc. Exp. Biol. Med. 124, 1316–1320.
Spector, R., Keep, R.F., Robert Snodgrass, S., Smith, Q.R., Johanson, C.E., 2015. A balanced view of choroid plexus structure and function: Focus on adult humans. Exp. Neurol. 267, 78–86.
Spijkerman, J.M., Geurts, L.J., Siero, J.C.W., Hendrikse, J., Luijten, P.R., Zwanenburg, J.J.M., 2018 May 9. Phase contrast MRI measurements of net cerebrospinal fluid flow through the cerebral aqueduct are confounded by respiration. J. Magn. Reson. Imaging. https://doi.org/10.1002/jmri.26181. [Epub ahead of print].
Thomas, C., Sadeghi, N., Nayak, A., Trefler, A., Sarlls, J., Baker, C.I., Pierpaoli, C., 2018. Impact of time-of-day on diffusivity measures of brain tissue derived from diffusion tensor imaging. NeuroImage 173, 25–34.
Tisell, M., Almstrom, O., Stephensen, H., Tullberg, M., Wikkelso, C., 2000. How effective is endoscopic third ventriculostomy in treating adult hydrocephalus caused by primary aqueductal stenosis? Neurosurgery 46, 104–110 (discussion 110-101).
Trefler, A., Sadeghi, N., Thomas, A.G., Pierpaoli, C., Baker, C.I., Thomas, C., 2016. Impact of time-of-day on brain morphometric measures derived from T1-weighted magnetic resonance imaging. NeuroImage 133, 41–52.
Tulassay, T., Khoor, A., Bald, M., Ritvay, J., Szabo, A., Rascher, W., 1990. Cerebrospinal fluid concentrations of atrial natriuretic peptide in children. Acta Paediatr Hung 30, 201–207.
Tumani, H., Huss, A., Bachhuber, F., 2018. The Cerebrospinal Fluid and Barriers - Anatomic and Physiologic Considerations. Handb Clin Neurol. Elsevier, pp. 21–32.
Virhammar, J., Laurell, K., Cesarini, K.G., Larsson, E.M., 2014. The callosal angle measured on MRI as a predictor of outcome in idiopathic normal-pressure hydrocephalus. J. Neurosurg. 120, 178–184.
Wagshul, M.E., Chen, J.J., Egnor, M.R., McCormack, E.J., Roche, P.E., 2006. Amplitude and phase of cerebrospinal fluid pulsations: experimental studies and review of the literature. J. Neurosurg. 104, 810–819.
Xie, L., Kang, H., Xu, Q., Chen, M.J., Liao, Y., Thiyagarajan, M., O'Donnell, J., Christensen, D.J., Nicholson, C., Iliff, J.J., Takano, T., Deane, R., Nedergaard, M., 2013. Sleep drives metabolite clearance from the adult brain. Science 342, 373–377.
Yildiz, S., Thyagaraj, S., Jin, N., Zhong, X., Heidari Pahlavian, S., Martin, B.A., Loth, F., Oshinski, J., Sabra, K.G., 2017. Quantifying the influence of respiration and cardiac pulsations on cerebrospinal fluid dynamics using real-time phase-contrast MRI. J. Magn. Reson. Imaging 46, 431–439.